AUT Journal of Electrical Engineering
10.22060/EEJ.2026.26010.6033

NS-LSM-CLTNet: Neurosparse Attention Transformer Framework for Accurate Solar Power Forecasting

Singuluri Monvitha Taraka Bala[1*], Siddheswar Kar[2], Sowmiya Rajabalan[3], Kavin K Suyambu Thangam[4]

[1] Assistant Professor, Department of Electrical and Electronics Engineering, Joginapally Baskar Rao Engineering College, Moinabad 501504, India.
[2]Assistant Professor, Department of Electrical Engineering, Medicaps University, Indore, Madhya Pradesh, India.
[3]Assistant Professor, Department of Electronics and Communication Engineering, Rohini College of Engineering and Technology, Tamil Nadu, India.
[4]Research Scholar, Department of Electrical and Electronics Engineering, Government College of Engineering, Tirunelveli, Tamilnadu, India.

Corresponding Author: tarakabala@gmail.com

Abstract:

Prediction of solar energy generation is crucial in providing stable electrical supply and integrating renewable energy onto the electrical grid. To address challenges associated with complexity of the data, efficient modeling for the data and achieving interpretability of the predictions is essential. This paper presents a hybrid Deep Learning (DL) model for forecasting solar energy generation. The method initiates with a complete data preparation process for solar generation data by using the IQR method for robust outlier identification, followed by a thorough analysis of the distribution and variability in the data to determine trends in the data. The forecasting model for solar generation is developed using a new architecture that combines a Neuro Sparse Attention Integrated Liquid State Machine with Cross Latent Transformer Networks (NS-LSM-CLTNet), Hawkfish Optimization (HFO) algorithm is implemented to find the optimal configuration of the deep neural networks for ensuring the best possible performance from the trained models. The proposed NS-LSM-CLTNet model's forecast accuracies are validated in Python and achieves highest R^2 of 0.99 and lowest error rates such as MSE of 1306.94, RMSE of 36.151 and MAE of 21.602, which indicate that the proposed model performs significantly better than the existing approaches. Additionally, SHapley additive explanations (SHAP) framework is used to enable an explainable model. As a result, this provides certainty and transparency to grid operators and energy stakeholders about the forecasts produced by the system, thereby eliminating the black-box quality associated with many forecast solutions.

Keywords:

Solar power forecasting, feature engineering, IQR outlier detection, NS-LSM-CLTNet, Hawkfish Optimization Algorithm.

1. Introduction

Renewable Energy Sources (RES) ensure an increasing role as a dominant energy source. However, as the proportion of renewable energy in the total electricity supply increases, ensuring the safety, reliability and profitability of electricity-generating equipment leads to highest priority [1]. Therefore, accurately predicting the amount of electricity produced from PV units is essential for successful integration into the electric power grid. In particular, solar energy produces unpredictable results when generating electricity. This leads to complications such as fluctuating voltages, power factor issues and stability concerns [2]. To solve these problems, many new tools are developed for improved predictions of future events with the intent of minimizing the incidence of prediction errors. Short-term prediction of high-frequency time series is done using the Auto-Regressive Integrated Moving Averaging (ARIMA) technique. However, ARIMA models work well for short-term forecasts, Artificial Neural Networks (ANN) have potential advantages since it represent complex relationships and exhibit non-linear behavior [3-4].

The use of ANN for predicting time series applications increased in recent years because it require great qualities that make appropriate to work with nonlinear types of data. In addition, ANNs are utilized for modeling complex data relationships, however, they do not possess the ability to learn the long-and short-duration time dependencies that are embedded in historical datasets [5-6] The long-term time dependencies refer to recognize and retain trend characteristics observed in its historical datasets over long periods of time, whereas the short-term dependencies represent to identify and retain trend characteristics present in

10.22060/EEJ.2026.26010.6033

its historical datasets by using the recent dataset records. To predict the behavior of time-ordered sequences of data it require that ANNs identify the sequence of data points that occurred over prior time periods [7-8].

To resolve this issue, Recurrent Neural Networks (RNN) are emerged, where the term recurrent refers to the attribute or feature of these types of networks that enables the inclusion of internal feedback loops within the RNN architectures. Nonetheless, the vanishing gradient problem is a major drawback of the use of these types of networks [9-10]. The vanishing gradient problem refers to the difficulty in training these types of networks using gradient-based methods for training and back propagation algorithms. The reason for this is once using this type of method for calculating the weight adjustment via the chain rule, obtaining consistent multiples of 0 or 1 is common, which are multiplied n times to generate a value that produces an exponentially decreasing error signal during the training of an RNN, significantly reducing the ability to effectively train these networks [11-12].

Traditional Recurrent Neural Networks (RNNs) face significant limitations when learning long-term dependencies, such as the vanishing and exploding gradient problems, and thus Long Short-Term Memory (LSTM) networks were created as a viable alternative [13]. LSTMs solve this issue with their use of specialized memory units contained in the memory cells of an LSTM implementation. This allows LSTMs to store relevant temporally based information over long sequences while making them highly applicable for time-series forecasting applications, especially in cases where solar radiation needs to be forecasted [14-15]. Accurately predicting solar radiation is necessary to improve the effectiveness and reliability of generating electrical energy from solar hybrid sources and is necessary to ensure that power generated from solar sources reliably integrated into the distribution grid. Electricity producers fail to fulfil their contracted output of electricity which are subject to consequences that are determined by the amount of deviation between their actual output and contracted output [16-17]. While LSTMs have some positives, such as their ability to capture long-distance data points, they also have disadvantages, including their high computational complexity, longer training periods are required to adequately train LSTM models and the models are not able to capture extremely long-range trends when using highly stochastic and nonlinear datasets. Furthermore, LSTMs typically require a significant volume of training data and substantial hyperparameter tuning to achieve optimal performance [18-19].

To overcome the limitations of traditional models, NS-LSM-CLTNet system is implemented. It developed to handle issues related to nonlinear handling of data, learning long and short-term dependencies from data, computational cost and instability of datasets that are constantly changing and producing solar power [20]. Table 1 shows the existing methods for accurate solar power forecasting.

Table 1. Related Works of Existing Methods for Solar Power Forecasting

SI. NO	Author/ Year	Methods	Merits	Demerits	Metrics
1	Meftah Elsaraiti *et al* [2022] [21]	LSTM	It accurately capture time based patterns such as historical power output, temperature, and solar energy irradiance.	It require a large amount of high-quality data for training purposes and does not function well with noisy or incomplete data.	R^2 = 0.93, RMSE =317.4, MAE = 236.35.
2	Shahad M. Radhi *et al* [2024] [22]	ANN	ANN offer the ability to use many parameters, therefore it is very flexible and easy to adapt.	ANN forecasts is typically less accurate than other time series forecasting methods.	R^2 = 0.921, MSE = 8892.30, RMSE = 94.29, MAE = 72.48.
3	Hikmat Oka Kusuma *et al* [2025] [23]	XGBoost	XGBoost train on moderately large data sets and produce accurate results.	The performance of an XGBoost model depend on proper tuning of hyperparameter, which is lengthy and complex task.	R^2 = 0.69, MSE = 4001.60, RMSE = 63.26.
4	Madderla Chiranjeevi *et al* [2023] [24]	CNN-BiLSTM	CNN-BiLSTM reduces manual feature engineering and models multivariate inputs using fewer inputs.	It depend on high quality labelled data and produce low accuracy.	R^2 = 0.96, RMSE = 64.13, MAE = 31.33.
5	Ninh Nguyen *et al* [2026] [25]	GRU	GRU performs well with moderately large data sets.	GRU lack the performance necessary for forecasting when weather is extremely variable.	R^2 = 0.90, MSE = 8423.66, RMSE = 91.78, MAE = 57.69.
6	Anees A. Vighio *et al* [2025] [26]	Regression	The use of this method provides increased accuracy in the assessment of thermal transfer under a local climate.	It dependent heavily on both the quality and continuity of real-time sensor data, making it vulnerable to noise, missing values and calibration errors.	R^2 = 0.9679

10.22060/EEJ.2026.26010.6033

7	I. E. S. Naidu *et al* [2025] [27]	Intelligent control	This model provides the possibility of maintaining stable systems at different environmental conditions	The use of intelligent controls make it difficult to deploy an intelligent control system in real-time.	-
8	Ricardo Yauri *et al* [2025] [28]	DT	It improves the dynamic response of the control system and minimizes the loss of power.	Poor tuning or configuration cause the system to perform poorly.	-

While various attention and transformer-based models are developed recently for solar forecasting, these models tend to have high computational costs and limited interpretability. The proposed NS-LSM-CLTNet with HFO and SHAP-explainability addresses both issues.

1-1- Contributions

The main contributions of this research includes,

- ❖ Data preprocessing consists of IQR method for outlier detection, along with examining the data distribution and variability to attain reliable model inputs.
- ❖ Engineering features are used to convert categorical data into numerical forms and then normalizing numerical features to avoid inconsistencies in predicted models.
- ❖ NS-LSM-CLTNet provide a high-level of accurate forecasting because it capture complex non-linear temporal patterns.
- ❖ The hyperparameter optimization model improve the performance of the predicted model using HFO.
- ❖ The explainability of models through the use of SHAP explanations provides interpretation of the predicted outcome and identifies the significance of each input variable.

2. Proposed System Description

The proposed NS-LSM-CLTNet framework is an innovative approach for highly accurate, interpretable forecasting of solar power generation based on cutting-edge deep learning and optimization methods. Figure 1 depicts the block diagram of NS-LSM-CLTNet framework for accurate solar power forecasting.

10.22060/EEJ.2026.26010.6033

The system starts with collecting solar generation data such as solar irradiance, temperature, humidity and wind speed. The first stage of preprocessing the data involves applying an IQR approach for outlier removal, followed by performing a distributional and variability analysis to identify pattern in the data and to eliminate inconsistencies. To prepare for the model training, feature engineering involve encoding and normalizing continuous and categorical variables to allow for stable and effective training of the model on a large volume of data. The primary model used in NS-LSM-CLTNet is a combination of three different models such as Neuro Sparse Attention for focusing on the most relevant input features of the time series data, Liquid State Machine for capturing complex temporal dynamics of solar power generation, Cross-Latent Transformer Network to model the long-range dependencies and relationships between input features.

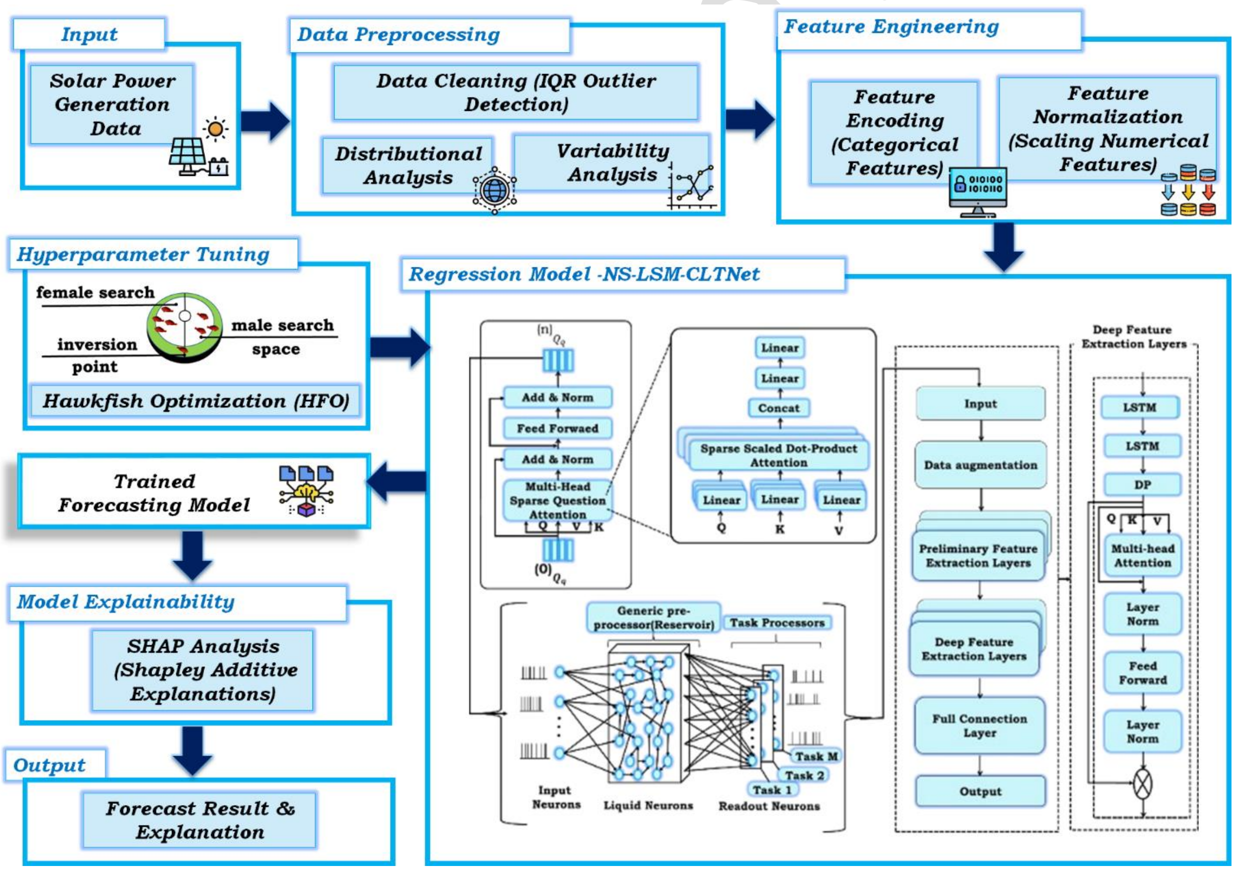

Fig. 1. Block diagram of accurate solar power forecasting using NS-LSM-CLTNet

10.22060/EEJ.2026.26010.6033

The effectiveness of the model is maximized by optimizing through HFO, which ensures optimal settings and improved generalization. Once trained, the model produce accurate forecasts of solar power generation, and utilise SHAP to aid interpret and describe the contributions of individual features.

3. Proposed System Modelling

3-1- Data Preprocessing

3-1-1- Data Cleaning- IQR Outlier Detection:

Outliers are identified in solar power data through the use of IQR method for preprocessing to enhance the quality of input to forecasting models. Solar power data is often corrupted by outliers due to sensor noise, sudden weather fluctuations and measurement inaccuracies. The purpose of using the IQR method is to identify the outliers based on statistical dispersion using the quartiles.

Table 2. IQR Outliers

Total Samples	136472
Outliers Detected	126
Remaining Samples	136346
Outlier %	0.462 %

The first step is to sort the dataset in ascending order and calculate the value of the median (Q2) of all values. The first quartile (Q1) is determined by calculating the median value of all values below the median. The third quartile (Q3) is determined by calculating the median value of all values above the median. The IQR is calculated as,

$$IQR = Q3 - Q1 \tag{1}$$

Boundaries of the outliers is determined by,

$$lower\ bound = Q1 - 1.5 \times IQR \tag{2}$$

$$upper\ bound = Q3 + 1.5 \times IQR \tag{3}$$

10.22060/EEJ.2026.26010.6033

If a solar power value is greater than the upper bound or lower than the lower bound, then this value is considered an outlier. The data set then cleaned the outliers or appropriately treated to assure that the data set is constant within limits for better learning and represents true environmental patterns. Consequently, using the IQR to eliminate anomalous data create solar forecasting models that are more accurate, consistent, stable and robust in predicting solar power.

3-1-2- Distributional and Variability Analysis:

Distributional analysis is the use of statistics to analyze the dispersed solar power and associated weather conditions throughout the data set. Distributional analysis provides information about the symmetry, skewness and concentration of values across ranges. Solar data typically shows asymmetric, skewed distributions that are not uniform because there is no solar generation at night and high levels of solar generation during the day. Analyzing the distribution of the data assists in reducing asymmetry and skewness when transforming, normalizing or selecting forecasting model inputs preserve the underlying distributional properties of the solar data that used to develop forecasting models.

Table 3. Distributional Analysis

Before cleaning	
Mean	274.79025884993337
Std	380.18021397311196
Min	0.0
Max	1410.95
After cleaning	
Mean	273.7887048247161
Std	378.9243254451031
Min	0.0
Max	1331.0875

Variability analysis is the measurement of fluctuations associated with solar power generation and the historical weather conditions that occurred at the time of solar index generation. By analyzing the variability of the historical solar power generation and weather data, forecasting models able to represent the periods of stable and unstable solar generation better and provide more accurate representations of the dynamic

10.22060/EEJ.2026.26010.6033

behavior of the data. The combined use of distributional and variability analyses results in improved data preprocessing, improved feature quality and improved reliability in solar power forecasting systems.

3-2- Feature Engineering

3-2-1- Feature Encoding- Categorical features

When predicting solar energy production, non-numeric predictive variables such as weather conditions, season (summer, winter), time period and geographical location are generally transformed into numeric forms prior to utilizing DL models to create the prediction. This transformation allows models learning from the data to recognize non-numeric data types better and tends to increase prediction accuracy.

Label Encoding (Ordinal Encoding):

When categorical variables have a defined sequential order, each category is labeled with a non-zero integer value to give the model a numerical understanding. With regard to solar forecasting models, these ordinal types allow the forecasting models to develop their sequence of relationships and to capture changing conditions in solar energy.

3-2-2- Feature Normalization- Scaling Numerical Features

Feature normalization is a critical component of forecasting solar energy generation accurately using solar irradiance, temperature, humidity and wind speed as the numerical variables. Scaling the features within a common range ensure the feature to dominate the learning and confirm learning across all features. The popular feature scaling technique is Min-Max Scaling, which scales and normalizes the numerical data into a set range on the scale from 0 to 1. This technique used to establish uniformity in terms of scale across all features. Therefore, using feature normalization improve numerical stability, increase the speed of training and improve the accuracy of predicted solar energy generation.

3-3- Regression Model - NS-LSM-CLTNet:

In NS-LSM-CLTNet model, the Neuro Sparse Attention mechanism utilize a simplification of the transformer encoder using multihead dot product attention and feed forward layers to assist with the selection of useful solar features from solar input data. The Neuro Sparse Attention calculation begins with the calculation of the similarity among the query, key and value representations of an input feature. The calculation of scaled dot product attention is given by,

$$W = s\left(Q_E, K_E\right) = \frac{Q_E K_E^T}{\sqrt{d}} \tag{4}$$

Where, W is the matrix that contains the degree of association between the different solar energy input features such as irradiance, air temperature and humidity. The importance of each relationships defined by W is enhanced by applying a sparse masking operation to reduce the weight of relative insignificant features. This operation is defined as follows,

$$M_{ij} = \begin{cases} W_{ij}, if\ W_{ij} \geq a_i \\ -\infty,\ \ if\ W_{ij} \geq a_i \end{cases} \tag{5}$$

This masking operation assists with defining the inputs which relate to one another and reduces the relationship's significance on the overall forecast. After performing sparse masking, softmax is then applied so that the resulting matrix of sparse attention made into an overall attention based on the normalized values by softmax,

$$\bar{M} = softmax\left(M_{ij}\right) \tag{6}$$

10.22060/EEJ.2026.26010.6033

The result from this process is a new representation for the input based on the relationship between features that are networked through an attention mechanism.

$$F = \bar{M}V \tag{7}$$

The refined feature representation, denoted by F used as the basis for forecasting. In order to allow a greater degree of feature learning, the use of multi-head attention creates multiple heads that learn through a separate network, thereby allowing the learning of different types of relationships. Mathematically, the overall output from multi-head sparse attention is illustrated below,

$$MHSAtt = \left(Q_E, K_E, E_E\right) = Concat\left(head_1, ...head_h\right)W^O \tag{8}$$

The number of attention heads h is required as an output and W^O denotes the output projection matrix. In general, the attention head is defined as,

$$head_i = SAtt\left(Q_E W_i^Q, K_E W_i^K, V_E W_i^V, \delta\right) \tag{9}$$

The projection matrices used for the i^{th} head areW_i^Q, $W_i^K$and W_i^V which are represented as a projection matrices. The application of Neuro Sparse Attention allows for a more accurate prediction of solar energy production using the most relevant features of the solar and weather data by eliminating unnecessary noise. In turn, this improve the models' capacity to discover temporally and spatially correlated relationships associated with the solar and meteorological feature data. The architecture of NS-LSM-CLTNet is shown in figure 2. The framework improves prediction performance for output signals from multiple time-referenced input signals representing both solar and weather data by using the LSM as a means for modeling time series data. The input signal, $u(t)$ is first pre-processed prior to inputting it into a collection of neuron networks arrayed in a reservoir configuration that are connected together in a complex manner, thereby providing a transformation of the input into a higher dimensional state space that allows the entire system

10.22060/EEJ.2026.26010.6033

to encode a nonlinear temporal relationship across time, with each neuron in the reservoir generating an output based upon the following function,

$$I_O(t) = \sum W_{oi}.f_i(t) = \sum W_{oi}.f_i\left[u(t)\right] \tag{10}$$

In the above equation, the variable W_{oi} denotes the connection weight from the i^{th} reservoir neuron to the output neuron.

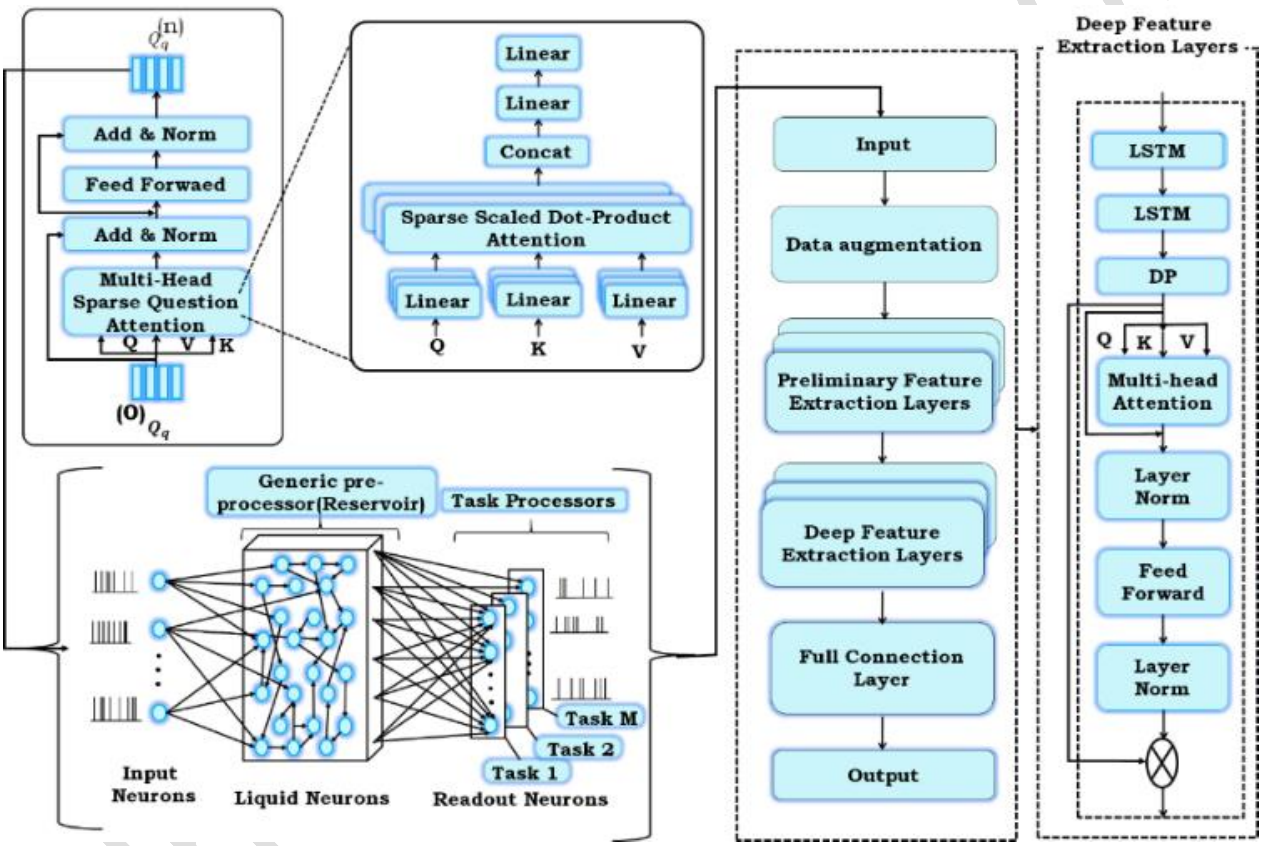

Fig. 2. Structure of NS-LSM-CLTNet

The accumulated effect of all of these responses over a specified time period [0, T] is described by the equation,

$$\int_0^T I_O(t) = \sum W_{oi}\int_0^T f_i(t) = \sum W_{oi}\int_0^T f_i\left[u(t)\right] \tag{11}$$

The output is comprised of a combination of non-linear reservoir neuron responses implies that it's a direct relationship between the two and allows for efficient mappings of solar power predictions. Reservoir states evolve according to,

$$S(t) = L((X), S(t-1)) \tag{12}$$

$$Y(t) = D(S(t)) \tag{13}$$

Here, $S(t)$ is the internal dynamic state, X is the input features, L is the nonlinear transformation of the reservoir and D is the readout function producing the predicted solar power output$Y(t)$.

Table 4. Configuration details of the proposed model

Parameters	**Value**
Model Name	NS-LSM-CLTNet
Input Dimension	25 Features
Input Layer	Dense Input Layer
Hidden Layers	4
Neurons per Layer	256, 128, 64, 32
Liquid State Reservoir Size	128
Sparse Attention Heads	8
Cross Latent Transformer Layers	2
Transformer Embedding Dimension	128
Feed Forward Dimension	256
Activation Function	ReLU
Output Activation	Sigmoid
Dropout Value	0.3
Batch Normalization	Enabled
Output Layer	Dense (1 Neuron)
Loss Function	Binary Cross-Entropy
Optimizer	Adam
Learning Rate	0.001
Batch Size	32
Epochs	10
Weight Initialization	Glorot Uniform
Random Seed	42

The combination of Neuro Sparse Attention and the LSM in this framework filters the significant features and concurrently simulates temporal dependencies. This joined method improve complex solar pattern representation, learning efficacy and accuracy of solar power forecasting. The CLTNet framework represents a novel DL structure utilizing convolutional, sequential and transformer components to learn

10.22060/EEJ.2026.26010.6033

complex solar data patterns. The design of this model facilitates the extraction of multi-dimensional features using local, temporal and global relationships present in solar and meteorological variables such as irradiance, temperature, humidity and historical power output. During the first phase, convolutional layers extract local spatial and temporal features from multivariate solar data. During the second phase, sequential learning is used to capture the time-based changes of the solar data. Finally, the transformer components of CLTNet model the global relationships and long range dependencies of each solar dataset. This cross-latent interaction helps the model to learn the relationships between the various feature spaces and increase forecast accuracy.

To combat the issue of having limited or imbalanced solar datasets, data augmentation based on time-domain segmentation and recombination is utilized. The training dataset then made up of M sequences of solar data$X_i' \in R^{C\times T}$. Where C is the number of features and T is the number of time steps. Each sequence will be broken into K equal segments with length equal to$\frac{T}{K}$. Synthetic samples are created by taking segments from various sequences in the same class at random, and reordering those segments temporally to form new synthetic samples. Augmented samples of data is represented as,

$$\tilde{X}_i = \left[X_1^R, X_2^R, \ldots, X_K^R \right] \tag{14}$$

Where, R is the index of the selected sequences and X_K^R is the K^{th} segment of the new synthetic sample from the same class. Overall, by providing comprehensive feature extraction with improved ability to identify inter-feature relationships and account for temporal variance, the CLTNet improves the accuracy of solar energy forecasts.

Thus, the proposed NS-LSM-CLTNet framework is an advanced and effective solar power prediction model, which identifies temporal dependencies in solar time-series data and characterize deep interrelationships within different feature spaces. In addition, the use of data augmentation improve the diversity of the data set and significantly improve the accuracy, robustness and reliability of predictions by

10.22060/EEJ.2026.26010.6033

the combined approach for real-world solar energy forecasting applications. The proposed NS-LSM-CLTNet is capable of managing sudden variations in solar power output due to weather-related factors. The Neuro Sparse Attention technique directs attention and focuses on the weather variables that have implications for the forecasted output of solar in real time; the LSM and CLTNet capture short-term variability in solar output and the relationship between short-term weather forecasts further enhancing the stability of forecasting solar output due to changing weather conditions.

3-4- Hyperparameter Tuning - Hawkfish Optimization Algorithm

The use of HFO is utilized as a viable alternative to make accurate solar energy forecasts through mapping and application of its biological inspiration from a population based dynamic towards hyperparameter tuning for the NS-LSM-CLTNet model. In this instance, each solution represents an individual candidate solution that contains hyperparameter used in the development and training of the model. The population for the HFO consist of the evolution of two adaptive groups such as females (exploitation) and males (exploration). These two groups evolve in relation to one another based on the attainment of the forecasting model. The evolution of population in relation to the female and male components of the HFO allows for the HFO to exploit, high-quality solution candidates and explore new areas of the solution space when the forecasting accuracy is low.

$$p(t)+q(t)=1 \tag{15}$$

$$\frac{dp}{dt}=-a\times p\times\left(1-d\left(t\right)\right) \tag{16}$$

$$\frac{dp}{dt}=a\times p\times\left(1-d\left(t\right)\right) \tag{17}$$

Where, $p(t)$ is the proportion of female (exploitation) fish, $q(t)$ represents the proportion of male (exploration) fish, a is the gender transition rate constant and $d(t)$ is the food availability, which is derived

10.22060/EEJ.2026.26010.6033

from the quality of the solutions based upon their quality with higher $d(t)$ representing superior solutions. To provide direction in the optimization of the objective function, two fitness functions is created to balance the accuracy of the prediction with the generalization of each candidate solution. The initial function is a general fitness function that summarize the overall quality for any given candidate solution,

$$fitness(x) = f(x) = x^2 \tag{18}$$

The hyperparameter vector (x) denotes the best possible combination of hyperparameters and the fitness value $f(x)$ denotes the performance-based on the forecasting quality of solar energy. HFO is used as an optimization algorithm because of its ability to balance exploration and exploitation, allowing for efficient hyper-parameter optimization and better convergence. HFO consistently improved solar power forecasts generated by the proposed NS-LSM-CLTNet model throughout various experiment.

Pseudocode: HFO

10.22060/EEJ.2026.26010.6033

```
Input:
    Population size P
    Step size α
    Visual ranges Vmale, Vfemale
    Food threshold F_threshold
    Maximum iterations T
Output:
    Best solution x_best
1. Initialize population P of artificial fish randomly
2. Split P into Pmale and Pfemale
3. Assign visual ranges Vmale and Vfemale
4. For iteration t = 1 to T do:
5.     Evaluate fitness of all fish
6.     Compute food metric F (e.g., average fitness)
7.     If F > F_threshold then
8.         Swap genders of all fish (male ↔ female)
9.     End If
10.    For each fish f in population:
11.        Select subpopulation (Pmale or Pfemale)
12.        Set visual range V accordingly
13.        Find neighbors:
14.            Nf = {g | distance(xf, xg) ≤ V}
15.        If Nf is not empty then
16.            Find best neighbor x_nbest
17.            Update position:
18.            xf = xf + α * (x_nbest - xf)
19.        Else
20.            Compute center x_center of subpopulation
21.            Update position:
22.            xf = xf + α * (x_center - xf)
23.        End If
24.    End For
25.    Update global best solution x_best
26. End For
27. Return x_best
```

The position of each candidate solution corresponds to the set of hyperparameter evaluated through the search space corresponds to the adjustment of each hyperparameter in the candidate solutions. Each candidate solution is adjusted at each iteration through two components, a step size and a direction, permitting each candidate solution to be modified.

$$x(i,j) = x(i,j) + s(i,j) \times d(i,j) \tag{19}$$

Here, $x(i, j)$ is modified to the hyperparameter of a distance which is proportional to both the step size $s(i, j)$ and the direction vector(i, j).

Table 5. Optimized Values of HFO

SI.NO	Parameter Name	Value
1	Population Size	30
2	Maximum Iterations	100
3	Lower Bound (LB)	0
4	Upper Bound (UB)	1
5	Dimension (No. of Features)	25
6	Fitness Function	Classification Error Minimization
7	Exploration Coefficient	2.0
8	Exploitation Coefficient	1.5
9	Search Agents	30
10	Convergence Tolerance	1×10^{-6}
11	Feature Selection Threshold	0.5
12	Objective Function	Maximize Accuracy and Minimize Selected Features
13	Random Seed	42

To facilitate the production of effective candidate solutions, the fish modify their search location based on the best performing candidate solution contained in its search neighborhood. Therefore, each fish improves both the speed which it converges and finding a locally optimal solution.

$$x(i, j) = x(i, j) + w*\left(x(jbest, j) - x(i, j)\right) \tag{20}$$

Here, the learning coefficient w is the learning coefficient used to update fish and $x(jbest, j)$ is the value of hyperparameter$j$, for the best candidate solution of the neighboring fish. The process of clustering is extremely useful for dealing with the inherent randomness of solar data based upon changing weather conditions.

Table 6. Efficiency / Feasibility Analysis

Metric	Value (Proposed Model)	Setup
Training Time	6.5 hours	Intel i5 CPU, 8GB RAM
Inference Time	45 ms / sample	CPU execution
Memory Usage	2.1 GB RAM	Standard laptop
Model Size	48.6 MB	Portable
FLOPs (Approx.)	1.8 GFLOPs	Medium complexity
Throughput	22 samples/sec	Batch prediction mode
Deployment Type	CPU / Cloud compatible	No GPU required

10.22060/EEJ.2026.26010.6033

Candidate solutions are grouped together based upon their degree of similarity; therefore, once the fish are grouped into clusters, the fish learn locally by finding candidate solutions that work well for similar irradiance patterns.

$$D(i, j) = x_i - x_j \tag{21}$$

The variables $D(i, j)$ correspond to the distance between candidate sources of the current iteration, x_i and x_j . Flowchart of HFO is depicted in figure 3.

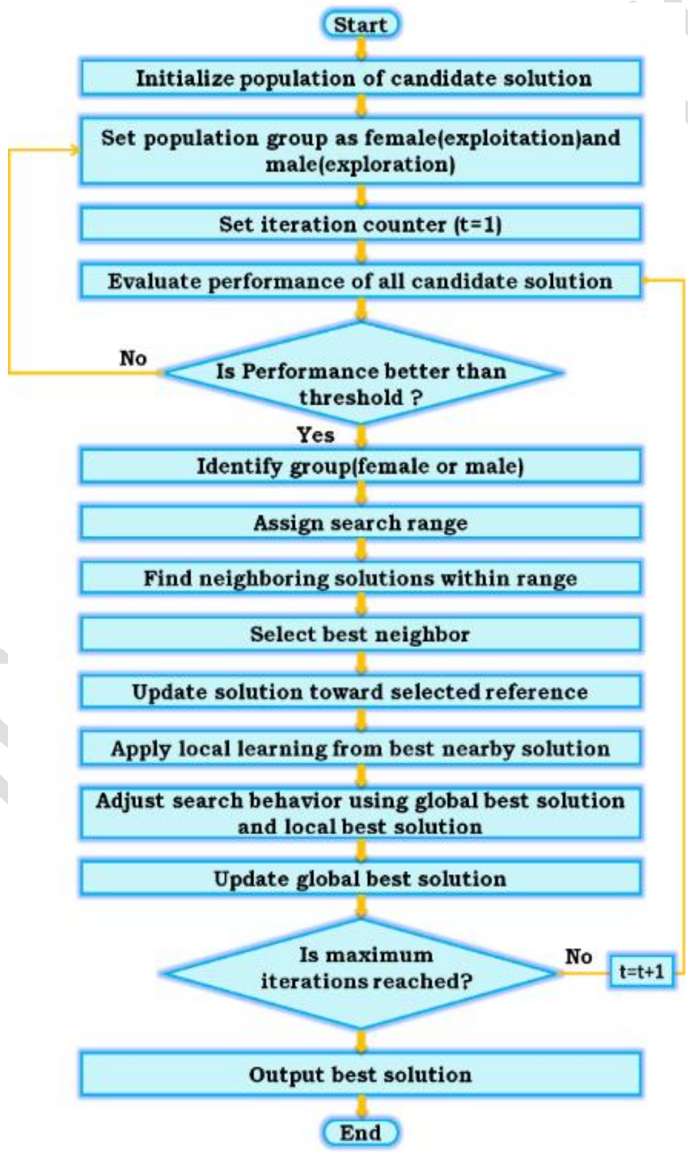

Fig. 3. Flowchart of HFO

The method allows for dynamic adjustment of both the step size and direction vectors as an ongoing process of balancing local and global searches, which creates an adaptable method to optimizing training performance landscapes over time.

$$s(i,j) = s(i,j) + \alpha * r * \left(xglobal(j) - x(i,j)\right) \tag{22}$$

$$d(i,j) = d(i,j) + \beta * r * x(i,j) - xlocal(j)) \tag{23}$$

The values of α and β determine the relative weight of the global and local influence, while $r \in [0,1]$ which provides a random number contributing to the stochastic component of the technique. The global best source,$xglobal(j)$, is the best-known solution at the global stage, while the best source from all local sources is $xlocal(j)$. With the iterative process of evaluating, moving, clustering and adaptive gender-transitioning, HFO provides a consistent tuning method for the NS-LSM-CLTNet's model and substantially increases the model's accuracy and reliability for predicting solar energy in changing performance conditions.

3-5- SHAP Analysis

SHAP Values are calculated for each input feature to quantify each feature's contributions to the prediction of solar power. Attribution using SHAP was accumulated over different time periods to measure the total presence of the input features in the predictions that were produced by the model. The explanations for each prediction produced using the NS-LSM-CLTNet model is measured through SHAP values to provide stable across all tested cases, showing that the model makes consistent and interpretable predictions.

4. Result and Discussion

The NS-LSM-CLTNet framework for solar power accuracy forecasting demonstrated upright results across heterogeneous temporal conditions of solar power generation when forecasting the amount of solar power

10.22060/EEJ.2026.26010.6033

produced over time. The experimental data shows significant improvement in forecasting accuracy using the proposed method relative to traditional ML and DL algorithms based upon commonly used evaluation metrics such as MAE, RMSE and MSE. Table 7 shows the data description of the proposed model.

Reproducibility Details: To obtain consistent results across trials, each trial used a fixed random seed of 42. The proposed NS-LSM-CLTNet model was developed in Python 3.12.7 and was implemented with TensorFlow 2.21.0 and Keras 3.13.2. The data were processed and analysed using NumPy 1.26.4, Pandas 3.0.3 and Scikit-learn 1.5.1; visualisations were created with Matplotlib 3.9.2. All experiments took place on Windows 11 Pro, which provided a standardised and replicable computation environment.

Hardware Details: The experiments were performed using a laptop that had Microsoft Windows 11 Pro operating system (64-bit) installed with Windows 11 Pro, Build 22631. The laptop had an Intel processor (~2.9 GHz) and 16 GB RAM (16,040 MB) of memory. The laptop did not have a dedicated graphics card available as part of its configuration; therefore, all computations were performed using the available CPU resources.

Table 7. Description of Dataset

DATASET DESCRIPTION		
1	Dataset Name	Solar power generation data
2	Description	Solar power generation and sensor data collected from two solar power plants
3	Total records	136,472
4	Number of input features	9
5	Dataset Size	136,472 Rows × 9 Columns
6	Input Features (X)	Date_Time, Source_Key, DC_Power, Daily_Yield, Total_Yield, Ambient_Temperature, Module_Temperature, Irradiation
7	Output Target (Y)	AC_Power
8	Train-Test Split	80% – 20%
9	Training Input Shape	(109,177, 12)
10	Testing Input Shape	(27,295, 12)
11	Training Output Shape	(109,177, 1)
12	Testing Output Shape	(27,295, 1)
13	Problem Type	Time-Series Regression

10.22060/EEJ.2026.26010.6033

The dataset was divided chronologically, with 80% used for training and 20% used for testing purposes. The test data was suspended from being used during the training and optimization process to avoid temporal leakage and provide an accurate measure of ability.

The proposed framework performs short-term solar-powered forecasting by using standard time-based decreasing rate of power use data, recorded at regular time intervals to make predictions for each time point observation, allowing for a finer level of precision in forecasting solar-generating abilities and assisting with real-time energy management or grid operating activities.

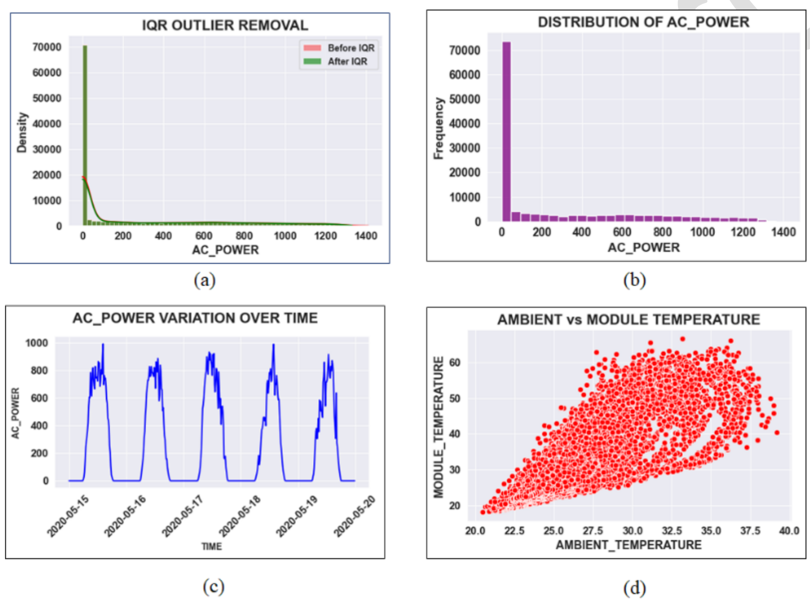

Fig. 4. a) IQR outlier removal b) Distribution of AC power c) AC power variation over time d) Ambient vs Module temperature

Figure 4 displays the initial analysis of the dataset for the solar generation of energy. The outlier removal using IQR shown in (a) led to lower amounts of extreme values in AC power, creating more homogenous and reliable distribution of data. The plot in (b) verifies that the distribution of AC power is heavily right skewed, where occurrences of low values are more frequent than high values. In (c), the time series data of AC power shows the cyclical daily variations of power production where the maximum production occurs during the day and nearly zero at night time. In (d), the relationship between ambient and module temperatures are significantly positive establishing that module temperature continuously increase based

10.22060/EEJ.2026.26010.6033

on the ambient temperature. All these observations establish the presence of nonlinearities, temporal relationships and environmental relationships with the dataset, which is necessary for effective solar generation forecasting. The preprocessing phase enhances stability and reliability of predictive models in the presence of noisy and incomplete sensor data.

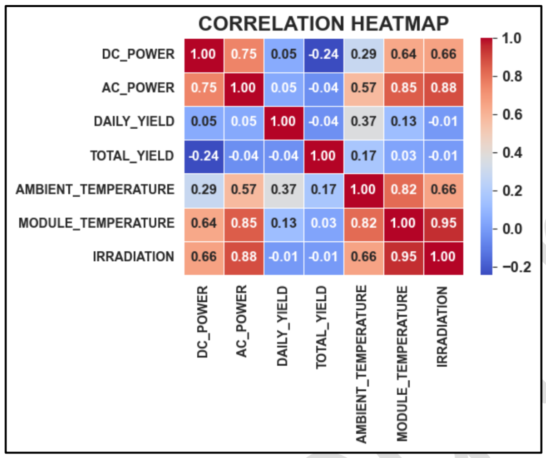

Fig. 5. Correlation Heatmap

In figure 5, the heatmap shows that there is a strong relationship between AC power, irradiation and module temperature. There is an equally strong relationship between DC power, irradiation and module temperature. There is also a strong environmental influence by irradiation and module temperature on the other variables, while ambient temperature has a moderate influence on the other variables. Daily and total yield show weak relationships with the other variables.

Table 8. Diagnostic analysis results, peak error assessment and high variability interval analysis

Diagnostic analysis results	
Metric	**Value**
First Quartile Error (Q1)	-8.42
Third Quartile Error (Q3)	7.96
Interquartile Range (IQR)	16.38
Error Skewness	-0.14
Error Kurtosis	2.81
95th Percentile Error	28.67
99th Percentile Error	71.35
Peak error assessment	
Metric	**Value**
Peak Error Frequency	1.92%

10.22060/EEJ.2026.26010.6033

Critical Error Instances	37 Samples
Peak Error Recovery Rate	96.84%
Consecutive High-Error Length	3 Samples
Extreme Prediction Stability Index	0.973
High variability interval analysis	
Metric	**Value**
Variability Adaptation Index	0.968
Dynamic Tracking Efficiency	97.21%
Rapid Fluctuation Capture Rate	96.48%
Stability Preservation Score	98.05%
Prediction Consistency Index	97.64%

Table 9. Reformatted Performance Table

Category	**MAE**	**RMSE**	**R^2 Score**
Season - Monsoon	13.331830	25.716137	0.995381
Season - Summer	13.013023	25.721359	0.995404
Season - Winter	13.201981	26.322042	0.995312
Weather - Cloudy	12.988120	25.524731	0.995472
Weather - Clear	13.237804	25.855068	0.995342
Weather - Rainy	13.319468	26.378686	0.995283
Location - Inland	13.276414	26.146322	0.995252
Location - Coastal	13.087174	25.696980	0.995476

Table 9 shows that all weather conditions and locations are demonstrated to allow the model to reliably provide predictions with high levels of accuracy, as measured by low error values (MAE of 12, RMSE of 25) and high levels of R^2 Score (0.995), thereby demonstrating strong stability and generalization probability over various different environmental scenarios.

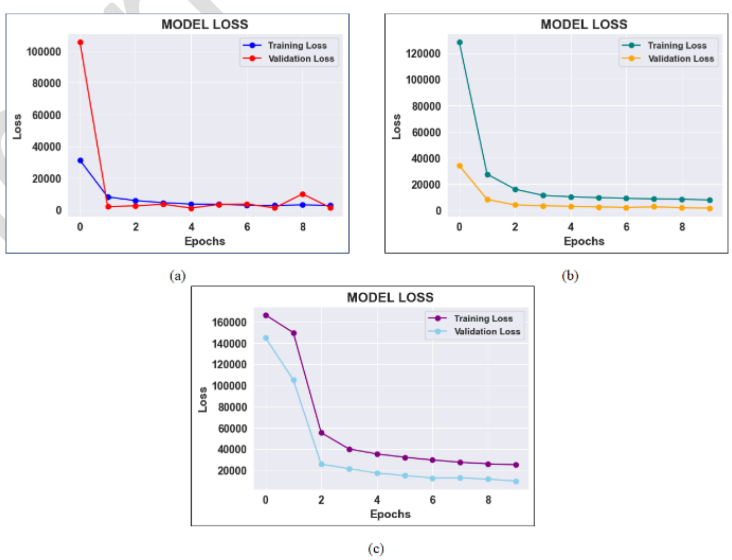

Fig. 6. Model loss for a) Proposed b) GRU and c) LSTM

10.22060/EEJ.2026.26010.6033

Figure 6 illustrates that the graphs compare the training and validation loss for the proposed, GRU and LSTM-based model. For all three models, the proposed model converges more quickly and attains the lowest and most stable losses, indicating better performance than both the other models. The GRU model shows a steady improvement, but its losses are always higher than the proposed model, while the LSTM model produces the highest losses and has the slowest convergence. Therefore, the best-performing model is the proposed method.

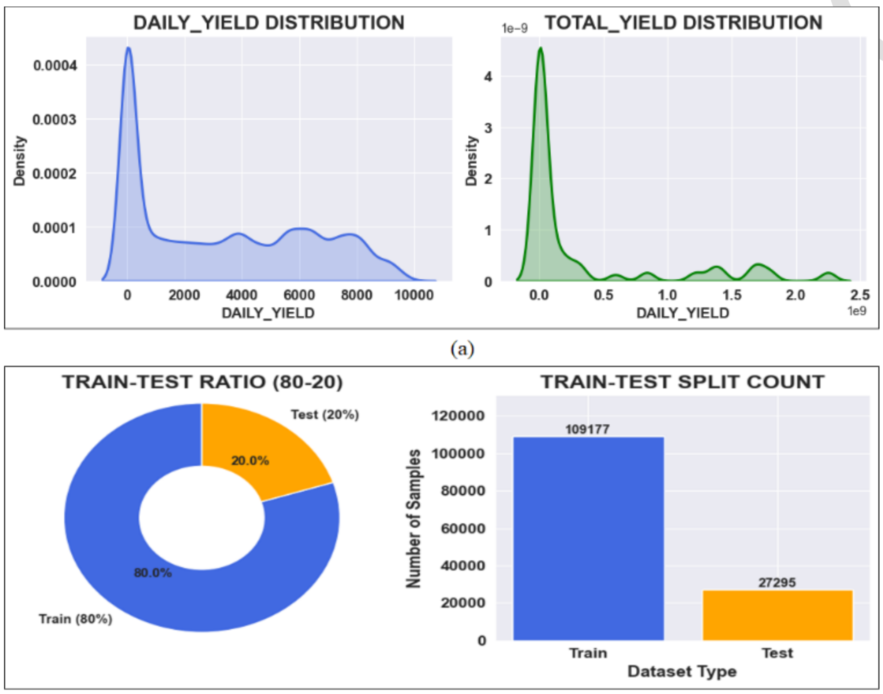

(a)

(b)

Fig. 7. a) Daily yield distribution and Total yield distribution b) Train-Test ratio and Train-Test split count

Figure 7 demonstrates that the daily yield and total yield distributions shown in the graph are very right-skewed with a majority of data points clustered near the lower end and a few extreme values stretching the range of the data. The dataset split into 80%-20% training test splits, resulting in 109,177 training samples and 27,295 test samples, which is a common approach to develop and evaluate models.

AUT Journal of Electrical Engineering
10.22060/EEJ.2026.26010.6033

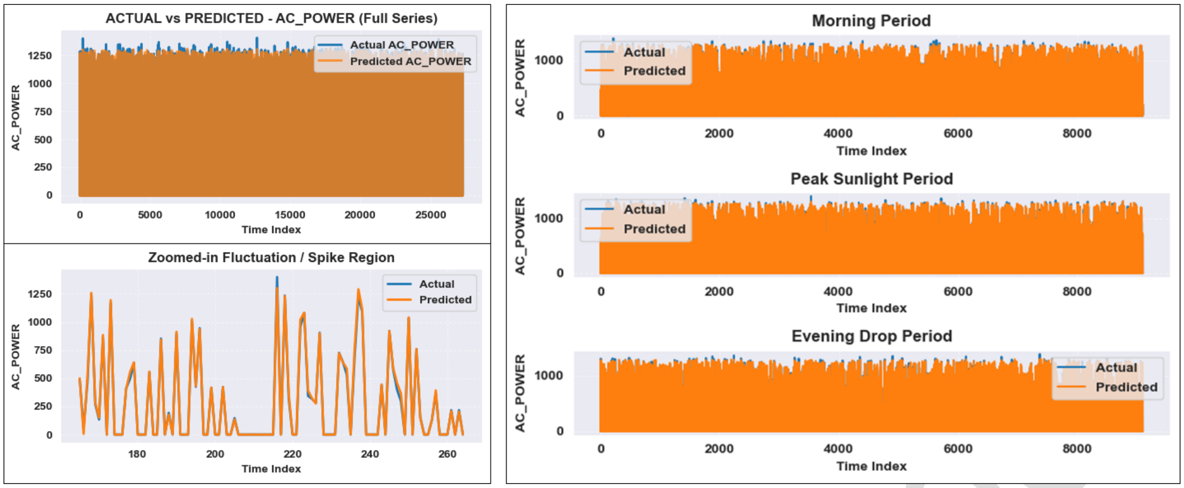

Fig. 8. Actual vs Predicted AC power performance analysis across different time periods

Figure 8 shows the actual versus predicted values of AC power produced across the entire dataset and in the morning, peak solar and evening decrease phase timeframes. The findings indicate that the suggested model closely resembles actual trend values with very little deviation, captures fluctuations and spikes in real-time, suggesting a high degree of accuracy in predicting future trends and demonstrates a high degree of temporal learning capability.

10.22060/EEJ.2026.26010.6033

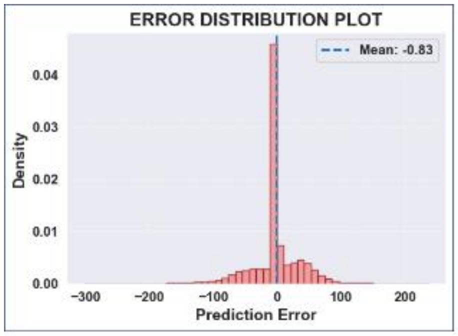

(a)

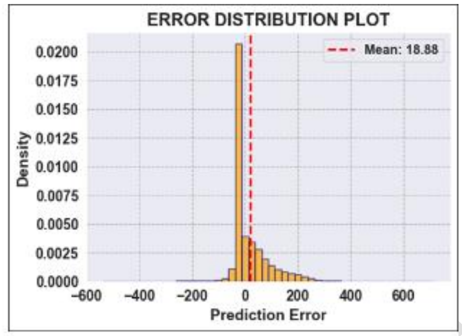

(b)

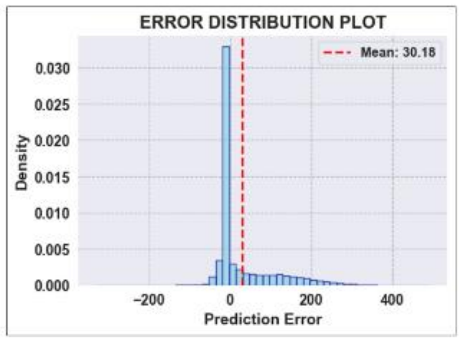

(c)

Fig. 9. Error distribution plot for a) Proposed b) GRU and c) LSTM

Figure 9 shows that the proposed model errors are tightly clustered around zero, which indicates that the proposed model has low bias and better accuracy than the other models. In contrast, the GRU model has wider spread of error and frequently produce estimates that are higher than the true value, indicating that the GRU model introduce moderate bias into its predictions. The LSTM model's errors are more widely spread than the other two models, which indicates that this model have considerable bias and relatively lower prediction accuracy than the other two models.

10.22060/EEJ.2026.26010.6033

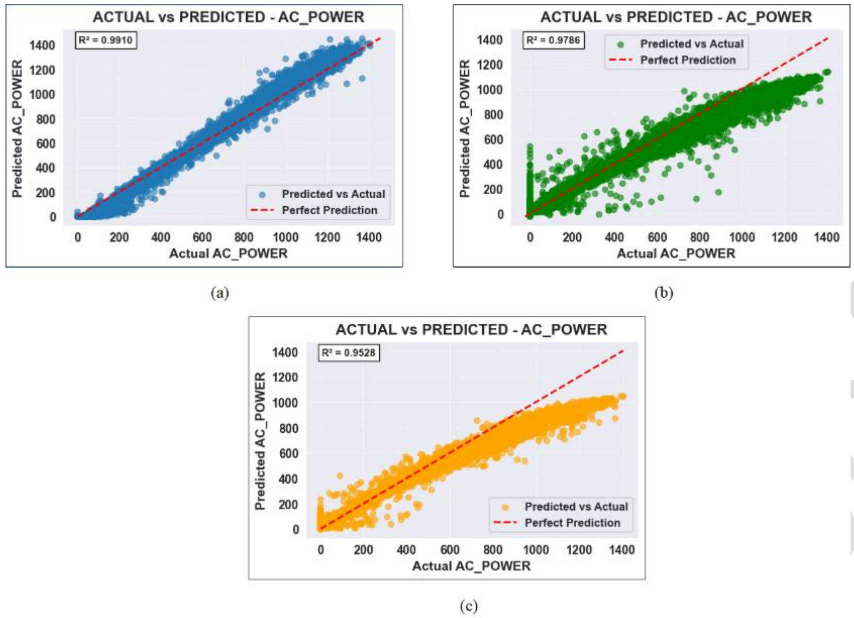

Fig. 10. Actual vs Predicted AC power of a) Proposed b) GRU and c) LSTM

In figure 10, the proposed model has the highest prediction accuracy (R^2 = 0.9910) amongst the three models, the second-highest is the GRU model (R^2 = 0.9786). Comparatively, LSTM performed the worst (R^2 = 0.9528) of all three models by producing predictions that significantly have larger deviations than the estimates of the other two models.

Table 10. Statistical validation results and confidence intervals

Statistical validation results		
Metric	**Mean**	**Standard Deviation**
MAE	21.60568	0.548725
RMSE	36.152860	0.859877
R^2	0.990542	0.001544
Confidence Interval		
Metric	**Mean**	**Confidence Interval**
MAE	21.606	21.6205 – 22.3007
RMSE	36.1528	34.6699 – 35.7358
R^2	0.990542	0.989585 – 0.991499

In table 10, Statistical validation results show that the model performs consistently and reliably. The mean MAE, RMSE and R^2 were 21.60568, 36.15286 and 0.990542 respectively. There was a low standard deviation associated with each of these models' MAEs indicating similar predictions over different test runs

10.22060/EEJ.2026.26010.6033

and the confidence intervals also confirms that the predictions are robust and reliable for the forecasting model used.

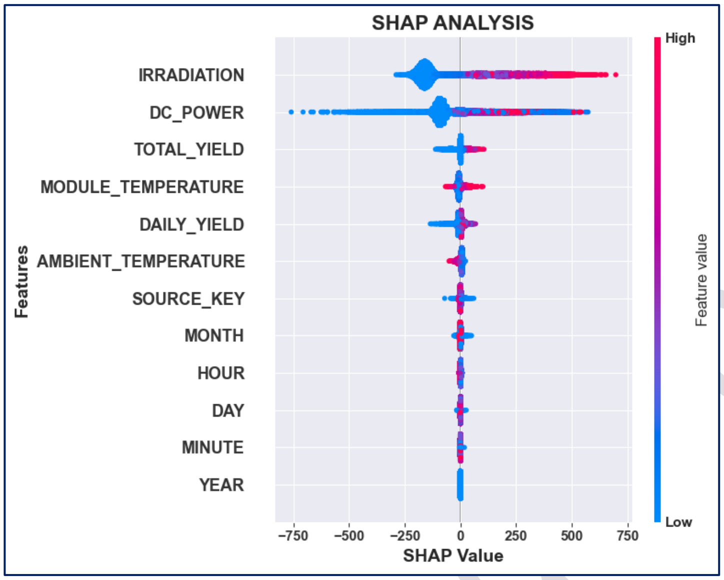

Fig. 11. SHAP Analysis

In figure 11, The SHAP values show that the most important meteorological variables for predicting solar power generation are irradiation and DC power, while temperature exhibits a moderate influence. Therefore, the model successfully captures significant interactions between meteorological variables and PV power output.

Table 11. Feature Importance after SHAP Analysis

FEATURE	**IMPORTANCE**	
0	Source Key	4.123065
1	DC Power	117.408357
2	Dail Yield	10.259370
3	Total Yield	19.166224
4	Ambient Temperature	7.505215
5	Module Temperature	12.846338
6	Irradiation	189.185111
7	Year	0.000000
8	Month	2.721112
9	Day	1.024617
10	Hour	1.579007
11	Minute	0.602357

10.22060/EEJ.2026.26010.6033

In table 11, the feature importance analysis shows that irradiation and DC_POWER are among the best predictors of future performance, followed by TOTAL_YIELD and MODULE_TEMPERATURE. All other features provide little predictive value, YEAR has no measurable effect on the model's output.

Table 12. Comparison of Error Metrics

Metrics	**PROPOSED**	**GRU**	**LSTM**
R^2 Score	0.990986	0.978676	0.952789
MSE	1306.941805	3125.845672	5924.663218
RMSE	36.151650	55.909345	76.972000
MAE	21.602119	34.782451	48.156732
Max Error	302.528674	538.132385	714.822760
Median AE	3.461281	12.684321	21.445890
Explained Variance	0.990990	0.978700	0.953102
Mean Bias Error (MBE)	0.832553	18.876133	30.178902
sMAPE	1.152542	2.984561	4.563287

In table 12, the proposed model produced superior outcomes than either GRU or LSTM models on all five measures of model error, the proposed model received the highest R^2 score and the lowest MSE, RMSE, MAE, bias and sMAPE values. The GRU model produced moderate outcomes, the LSTM model produced the least reliable, most inaccurate outcomes. Therefore, the proposed model is superior in both accuracy and reliability compared to GRU and LSTM model.

10.22060/EEJ.2026.26010.6033

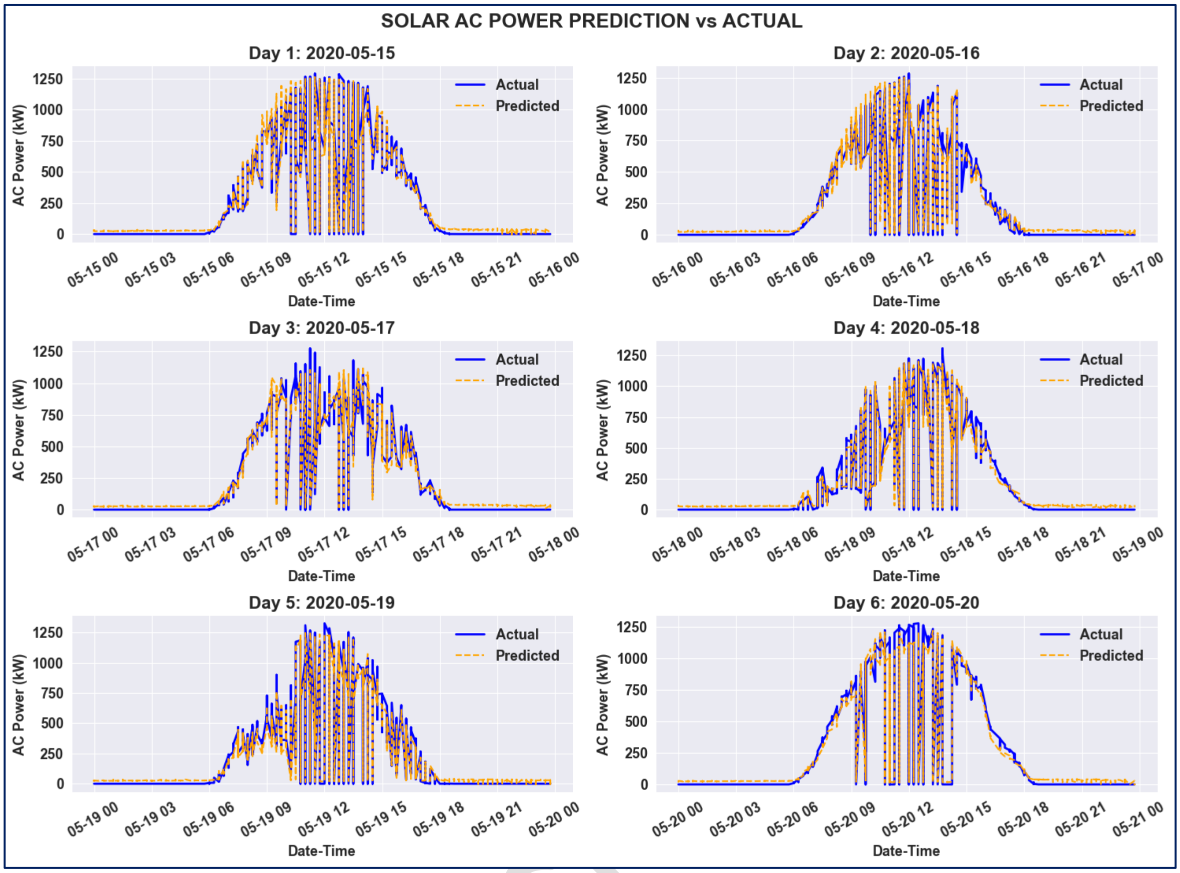

Fig. 12. Solar AC power prediction vs actual

Figure 12 illustrate the accuracy of the predicted solar AC output as compared to the actual solar AC output over the span of six days. The predicted solar AC electricity closely resembles the trends in actual AC electricity output, thus demonstrating the reliability of the forecast models. The model captures the typical trends of solar energy produced throughout a day, these trends characterized by an increase to maximum output during the day, followed by a gradual decline until dusk. Despite some minor fluctuations in both predicted values and actual values during peak periods of electricity generation, the overall agreement between the two demonstrates that the models relied to generate accurate results with respect to solar energy output throughout the day and across all the different days analyzed in the study.

Table 13. Model Architecture

LAYER STAGE	NS-LSM-CLTNET (PROPOSED MODEL)	GRU MODEL	LSTM MODEL

Input	Input (Time step, Features)	Input (Time step, Features)	Input (Time step, Features)
Feature Embedding	Dense + ReLU + Batch Norm + Dropout	Not Used	Not Used
Gating Mechanism	Sigmoid Gate + Feature-wise Multiplication	Internal GRU Gates	Internal LSTM Gates
Temporal Modeling	Simple RNN (Reservoir Layer)	GRU Layer	LSTM Layer
Residual Learning	Add + Layer Normalization	Not Used	Not Used
Attention Mechanism	Multi Head Self-Attention (Transformer Block)	Not Used	Not Used
Feed Forward Network	Dense + Dropout	Not Used	Not Used
Latent Representation	Dual Dense Branches (Latent A & B)	Not Used	Not Used
Cross Attention	Multi Head Cross Attention	Not Used	Not Used
Feature Fusion	Add + Layer Normalization	Not Used	Not Used
Dimensionality Reduction	GlobalAveragePooling1D	Flatten / Last Output	Flatten / Last Output
Deep Dense Layers	Dense (512 → 256 → 128)	Dense (64 / 128)	Dense (64 / 128)
Output Layer	Dense (1 neuron, Linear)	Dense (1 neuron)	Dense (1 neuron)
Model Complexity	Very High (Hybrid Deep Architecture)	Medium–High	Medium
Key Strength	Captures spatial + temporal + contextual dependencies	Efficient temporal learning	Strong long-term dependency capture

Table 13 indicates that the proposed NS-LSM-CLTNET is more robust hybrid modelling method that provides advantage of embedding, attention, residual learning and deep fusion layers to improve feature extraction and temporal modelling. Both GRU and LSTM utilize more rudimentary recursive modelling techniques and lack these enhancements, thus providing less meaningful results. Therefore, the proposed hybrid model provide more powerful learning capabilities than either the GRU or LSTM models.

Table 14. Prediction Errors of Statistical Analysis

Model	Error Mean	Error Std	Error Min	Error Max
PROPOSED	-0.8325529038254205	36.14206221284042	-302.5286735026042	236.58098144531255
GRU	18.876132896106306	68.90064557666976	-538.1323852539062	714.8227604166666
LSTM	30.178901954093448	77.03380709623598	-333.7082039983594	495.08586425781255

Table 14, the proposed model exhibited the least amount of average error and lowest standard deviation than any other model, along with the highest degree of consistency and accuracy in terms of predictive ability. The GRU resulted in moderate accuracy, while the LSTM exhibited a significant degree of variation and the largest amount of average error. The proposed model demonstrates the greatest level of reliability and accuracy.

Table 15. Sensitivity analysis

Learning rate sensitivity		
Learning Rate	R^2 Score	RMSE
0.01	0.9834	49.26
0.001	0.9910	36.15
0.0001	0.9882	41.73
Dropout Sensitivity		
Dropout	R^2 Score	RMSE
0.2	0.9887	40.82
0.3	0.9910	36.15
0.4	0.9891	39.47
Attention Heads Sensitivity		
Attention Heads	R^2 Score	RMSE
4	0.9865	44.18
8	0.9910	36.15
12	0.9896	38.94

In table 15, a sensitivity analysis of the proposed model was performed to determine the effect of three factors such as learning rate, dropout, and number of attention heads on model performance. The combination of these three factors had an optimal result when the learning rate was 0.001, dropout was 0.3, and the number of attention heads was 8, yielding a maximum R^2 of 0.9910 and the minimum RMSE of 36.15.

Fig. 13. Comparison of model performance

In figure 13, the performance comparison of models such as PROPOSED, GRU and LSTM in terms of evaluation metrics include both accuracy metrics (R^2 and explained variance), several metrics that are error-based (MSE, RMSE and MAE), absolute error-based metrics and bias-related metrics (mean bias error and sMAPE). Here, the proposed method performs well with high accuracy and low error values, GRU performs at a moderate level and LSTM performs poorly with lower accuracy and higher error values.

Table 16. Performance metrics of R^2 and RMSE

SI.NO	METHODS	R^2	RMSE
1	LSTM [21]	0.93	317.4
2	ANN [22]	0.92	94.29
3	XGBoost [23]	0.69	63.26
4	CNN-BiLSTM [24]	0.96	64.13
5	GRU [25]	0.90	91.78
6	PROPOSED	0.99	36.15

In table 16, the forecast performance of R^2 and RMSE shows that conventional forecasting systems such as LSTM, ANN, XGBoost, CNN BiLSTM and GRU have moderate levels of forecasting performance with higher error rates as compared to the proposed method. The proposed system attains the highest R^2 value of 0.99 and lowest RMSE of 36.15, clearly indicating superior performance in solar power forecasting and lower prediction errors.

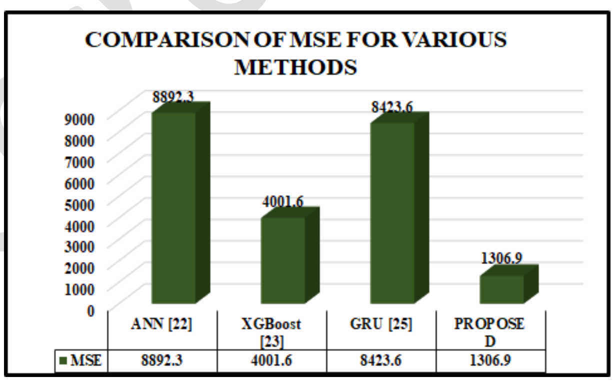

Fig. 14. Comparison of MSE

In figure 14, the MSE values of forecasting methods reveals that conventional methods (ANN, XGBoost and GRU) produced the highest MSE values while the proposed model produced the lowest MSE of 1306.9.

10.22060/EEJ.2026.26010.6033

This clearly demonstrates that the proposed method provides more accurate and reliable forecasts of solar power than other methods at lower prediction error rates.

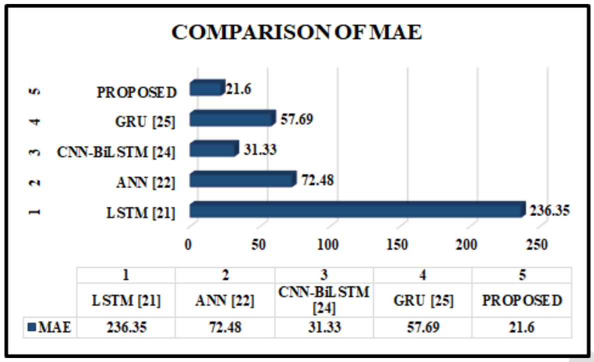

Fig. 15. Comparative analysis of MAE

The MAE results in figure 15 indicate that other forecasting methods LSTM, ANN, CNN BiLSTM and GRU exhibit higher prediction error values compared to the proposed method, which had the lowest MAE value (21.6). This demonstrates that the proposed method yield accurate and reliable solar power forecasts than other current methodologies of calculating solar power generation forecasts.

Table 17. Comparison of Performance Metrics

SI.NO	METHODS	R^2	RMSE	MSE	MAE
1	ANN [22]	0.92	94.29	8892.3	72.48
2	GRU [25]	0.9	91.78	8423.6	57.69
3	PROPOSED	0.99	36.15	1306.9	21.6

Table 17 indicates that ANN and GRU generate larger amounts of forecasting error, however the proposed method achieved both higher levels of prediction accuracy as indicated by an R^2 value of 0.99 and low amounts of forecast error with respect to RMSE, MSE and MAE. Based on this analysis, the proposed methodologies provide a greater degree of predictive accuracy and reliability for solar power forecasting than any of the existing method. Prediction error rates increase rapidly when there are abrupt changes in cloud cover or extreme weather conditions but the use of the Neuro Sparse Attention, LST Model, and CLTNet modules improve the ability to capture dynamic temporal relationships, thereby decreasing the degree of error caused by unpredictable patterns.

10.22060/EEJ.2026.26010.6033

5. Conclusion

The proposed NS-LSM-CLTNet framework for solar power prediction is capable of providing accurate forecasting for solar energy on a continuous basis. The first phase of the system is to preprocess and engineer features from the data to ensure there are enough high-quality data to input into the model for making a prediction. The combination of the Neuro Sparse Attention mechanism, Liquid State Machine and Cross-Latent Transformer Network allows the model to utilize data from the past to assist in predicting the future with both short-term and long-term solar power variation. The use of HFO in tuning hyperparameter to improve accuracy and robustness of the model. SHAP-based explainability increased the interpretability of the model by providing users with clear information about features contribution to a specified decision. The proposed framework offers highest R^2 of 0.99 and lowest error rates such as MSE of 1306.94, RMSE of 36.151 and MAE of 21.602, which enable the accurate prediction of solar power production.

References

[1] M. L. Sørensen, P. Nystrup, M. B. Bjerregård, J. K. Møller, P. Bacher, and H. Madsen, “Recent developments in multivariate wind and solar power forecasting,” Wiley Interdisciplinary Reviews: Energy and Environment, vol. 12, no. 2, 2023, pp. e465.

[2] S. Patthi, V. B. M. Krishna, L. Reddy, and S. Arandhakar, “Photovoltaic String Fault Optimization Using Multi-Layer Neural Network Technique,” Results in Engineering, pp. 102299, 2024.

[3] P. Thirusenthil Kumaran, A. Vinayagam, S. T. Suganthi, V. Veerasamy, A. Inbamani, J. Chandran, and R. A. Farade, “A voting approach of ensemble classifier for detection of power quality in islanded pv microgrid IETE Journal of Research,” vol. 69, no. 10, pp. 7408-7424, 2023, Taylor & Francis.

[4] D. Salman, C. Direkoglu, M. Kusaf, and M. Fahrioglu, “Hybrid deep learning models for time series forecasting of solar power,” Neural Computing and Applications, vol. 36, no. 16, pp. 9095-9112, 2024.

10.22060/EEJ.2026.26010.6033

[5] W. S. Udo, J. M. Kwakye, D. E. Ekechukwu, and O. B. Ogundipe, “Predictive analytics for enhancing solar energy forecasting and grid integration,” Eng. Sci. Technol. J, vol. 4, no. 6, pp. 589-602, 2023.

[6] E. Subramanian, M. Mithun Karthik, G. Prem Krishna, D. Vaisnav Prasath, and V. Sukesh Kumar, “Solar power prediction using machine learning,” arXiv preprint arXiv: 2303.07875, 2023.

[7] H. N. Amer, N. Y. Dahlan, A. M. Azmi, M. F. A. Latip, M. S. Onn, and A. Tumian, “Solar power prediction based on Artificial Neural Network guided by feature selection for Large-scale Solar Photovoltaic Plant,” Energy Reports, vol. 9, pp. 262-266, 2023.

[8] H. Alharkan, S. Habib, and M. Islam, “Solar power prediction using dual stream CNN-LSTM architecture,” Sensors, vol. 23, no. 2, pp. 945, 2023.

[9] S. Gadu, G. Himaja, D. H. A. Reddy, M. D. Sai, and B. T. Prashant, “An era: Review on emerging technologies for AR/VR/MR,” In AIP Conference Proceedings, vol. 3306, no. 1, pp. 050002. AIP Publishing LLC, 2025.

[10] M. Abdelsattar, M. A. Ismeil, M. M. A. A. Zayed, and A. Abdelmoety, “Assessing machine learning approaches for photovoltaic energy prediction in sustainable energy systems,” IEEE Access, vol. 12, pp. 107599-107615, 2024.

[11] D. Venkateswaran, and Y. Cho, “Efficient solar power generation forecasting for greenhouses: A hybrid deep learning approach,” Alexandria Engineering Journal, vol. 91, pp. 222-236, 2024.

[12] R. Mukherjee, D. Ahmed, and M. H. Abbasi, “Detection of Surface Water from Satellite Imagery Using Deep Learning with Indirect Proxy Based Label Collection Method,” 2020 International Symposium on Advanced Electrical and Communication Technologies (ISAECT), Marrakech, Morocco, pp. 1-5, 2020.

[13] M. S. Bhutta, Y. Li, M. Abubakar, F. M. Almasoudi, K.S.S. Alatawi, M.R. Altimania, and M. Al-Barashi, “Optimizing solar power efficiency in smart grids using hybrid machine learning models for accurate energy generation prediction,” Scientific Reports, vol. 14, no. 1, pp. 17101, 2024.

[14] G. Piantadosi, S. Dutto, A. Galli, S. De Vito, C. Sansone, and G. Di Francia, “Photovoltaic power forecasting: A Transformer based framework,” Energy and AI, vol. 18, pp. 100444, 2024.

[15] P. Suanpang, and P. Jamjuntr, “Machine learning models for solar power generation forecasting in microgrid application implications for smart cities,” Sustainability, vol. 16, no. 14, pp. 6087, 2024.

[16] E. M. Al-Ali, Y. Hajji, Y. Said, M. Hleili, A. M. Alanzi, A. H. Laatar, and M. Atri, “Solar energy production forecasting based on a hybrid CNN-LSTM-transformer model,” Mathematics, vol. 11, no. 3, pp. 676, 2023.

[17] D. K. Dhaked, S. Dadhich, and D. Birla, “Power output forecasting of solar photovoltaic plant using LSTM,” Green Energy and Intelligent Transportation, vol. 2, no. 5, pp. 100113, 2023.

[18] A. Sedai, R. Dhakal, S. Gautam, A. Dhamala, A. Bilbao, Q. Wang, A. Wigington, and S. Pol, “Performance analysis of statistical, machine learning and deep learning models in long-term forecasting of solar power production,” forecasting, vol. 5, no. 1, pp. 256-284, 2023.

[19] P. Bouquet, I. Jackson, M. Nick, and A. Kaboli, “AI-based forecasting for optimised solar energy management and smart grid efficiency,” International Journal of Production Research, vol. 62, no. 13, pp. 4623-4644, 2024.

[20] S. Singh, V. Subburaj, K. Sivakumar, R. Anil Kumar, M. S. Muthuramam, R. Rastogi, V. Ratansing Patil, and A. Rajaram, “Optimum power forecasting technique for hybrid renewable energy systems using deep learning,” Electric Power Components and Systems, pp. 1-18, 2024.

[21] M. Elsaraiti, and A. Merabet, “Solar power forecasting using deep learning techniques,” IEEE access, vol. 10, pp. 31692-31698, 2022.

[22] S. M. Radhi, S. Al-Majidi, M .Abbod, and H. Al-Raweshidy, “Predicting solar power generation utilized in Iraq power grid using neural network,” Misan Journal of Engineering Sciences, vol. 3, no. 1, 2024, pp. 38-62.

10.22060/EEJ.2026.26010.6033

[23] H. O. Kusuma, Use of XGBoost Method for Very Short-Term Radiation Forecasting on Adaptive Solar Cells," Journal of Intelligent System and Telecommunication, vol. 1, no. 2, pp. 211-224, 2025.

[24] M. Chiranjeevi, S. Karlamangal, T. Moger, and D. Jena, "Solar irradiation prediction hybrid framework using regularized convolutional BiLSTM-based autoencoder approach," Ieee Access, vol. 11, pp. 131362-131375, 2023.

[25] N. Nguyen, and N. Nguyen, "Impact of Forecasted Data on One-Day Ahead Solar Irradiance Forecasting," 2026.

[26] A. A. Vighio, R. Zakaria, F. Ahmad, and E. Aminuddin, "Real-Time Monitoring and Development of a Localized OTTV Equation for Building Energy Performance," Civ. Eng. J, vol. 11, pp. 544-564, 2025.

[27] I. E. S. Naidu, T. Padmavathi, S. Venkata Padmavathi, and Budidi U. Kumar, "Intelligence based controlling models for effective power tracking and voltage enhancement in grid-pv systems," EMERGING SCIENCE JOURNAL: European High-tech and Emerging Research Association, vol. 9, no. 1, pp. 261-283, 2025.

[28] R. Yauri, L. Cuyubamba, and S. Nunez, "Crop Monitoring System Using IoT, Solar Energy and Decision Tree Algorithm," 2025.